

IMPROVING THE UNIFORMITY OF THE GAMMA PRODUCTION RATE DISTRIBUTION WITH DEPTH IN A LARGE BIOLOGICAL SAMPLE FOR AN IVNAA FACILITY

by

Hashem Miri HAKIMABAD and Lalle Rafat MOTAVALLI

Received on January 26, 2009; accepted in revised form on June 7, 2009

The design studies related to a prompt γ -rays *in vivo* neutron activation analysis facility are described. The designs were based on two neutron sources: ^{252}Cf and $^{241}\text{Am-Be}$, four collimator materials: polyethylene, 5% boric-acid doped polyethylene, graphite, and the heavy water, two collimator shapes: pyramidal and rectangular, and two configurations: unilateral and bilateral. The aim of this work was improving the uniformity of the gamma production rate distribution with depth in a large biological sample. For the sample, a water phantom measuring 32 cm \times 16 cm \times 100 cm was simulated. The simulations were performed by MCNPX 2.4.0 Monte Carlo code. This study recommends the prompt γ -rays IVNAA facility in the bilateral configuration with graphite as a collimator material and $^{241}\text{Am-Be}$ as neutron source.

Key words: gamma production, water phantom, MCNPX code, activation analysis

INTRODUCTION

In vivo neutron activation analysis (IVNAA) has become the “gold standard” method for the measurement of certain body elements which are unique constituents of body components, *e. g.* nitrogen in protein and calcium in the skeleton [1-7]. IVNAA has been applied and continues to be applied as an appropriate method in the measurement of trace body elements or toxic ingested elements in individuals with simultaneous (prompt) or delayed counting [8-11]. One of the most effective parameters on the measurement accuracy is the uniformity of the gamma production rate distribution with depth, especially for large samples such as human body [12-15]. The uniformity is the most significant factor of measurement accuracy when whole body counting is performed. The activation rate depends dominantly to the thermal neutron flux. Ther-

mal neutrons are made from moderating the fast neutrons, emitted from the source, during collisions with the collimator material and body elements. The moderating is principally performed by elastic scattering from hydrogen atoms. Thermalisation and capture of neutrons in the body induces the prompt γ -rays which would be detected. If the neutron capture rate is greater than the thermalisation rate, the thermal neutron flux decreases with the depth of the body, while the activation rate and subsequent thermal neutron flux should be as uniform as possible. From this view, incident fast neutrons are necessary for large biological samples. But such fast beams usually cause high doses in the body and could be, consequently, unusable.

In the presented work, a prompt γ -rays IVNAA facility was simulated by MCNPX 2.4.0 [16] Monte Carlo code. The scope of the work was to find a facility configuration which improves the uniformity. To study the effects of neutron source type and collimator material and shape on the uniformity of activation rate, 24 different configurations were investigated.

MATERIALS AND METHODS

To improve the uniformity of the activation rate in a given sample, the appropriate incident neutron spectrum should be obtained. The incident neutron spectrum depends on the source type, collimator shape and

Nuclear Technology & Radiation Protection
Scientific paper
UDC: 539.125.52 : 519.245
DOI: 10.2298/NTRP0902119H

Authors' address:
Physics Department, School of Sciences,
Ferdowsi University of Mashhad, Iran

E-mail address of corresponding author:
mirihakim@ferdowsi.um.ac.ir (H. M. Hakimabad)

material properties. To study the effect of these parameters, the dose calculations were performed for two fast neutron sources: ^{252}Cf and $^{241}\text{Am-Be}$ and for four collimator materials: polyethylene (CH_2), 5% boric-acid doped polyethylene ($\text{CH}_2\text{-B}$), graphite (C), and the heavy water (D_2O). The production rate of neutron-induced photons (numbers per cm^3s) and thermal ($E < 0.5$ eV), epithermal ($0.5 \text{ eV} < E < 10$ keV), and fast neutron ($E > 10$ keV) fluxes was also computed as a function of depth in that part of the phantom which was exposed to the neutron source. Neutron fluxes were estimated per one source neutron. Two shapes of collimator were considered: pyramidal and rectangular.

Facility description

The schematic diagram of the prompt γ -rays IVNAA facility is shown in fig. 1. The collimator is the inverted, rectangular pyramidal void cast in the $40 \times 40 \times 60 \text{ cm}^3$ block which includes the collimator material. The neutron source is positioned at the apex of the 45 cm deep inverted pyramid. The collimator makes a $40 \times 20 \text{ cm}^2$ aperture at the level of the bed. The aluminum bed is centrally placed 50 cm above the source. A water phantom measuring of $32 \times 16 \times 100 \text{ cm}^3$ is placed centrally on the scanning bed. Two pairs of NaI(Tl) detectors are positioned bilaterally to the phantom. Since the neutron source is horizontally placed between two pairs of NaI(Tl) detectors, there is no vertical cross-section of the facility which contains the source and the detector simultaneously. So, the neutron source is shown at the apex of the pyramidal collimator void hole designated with the dotted lines.

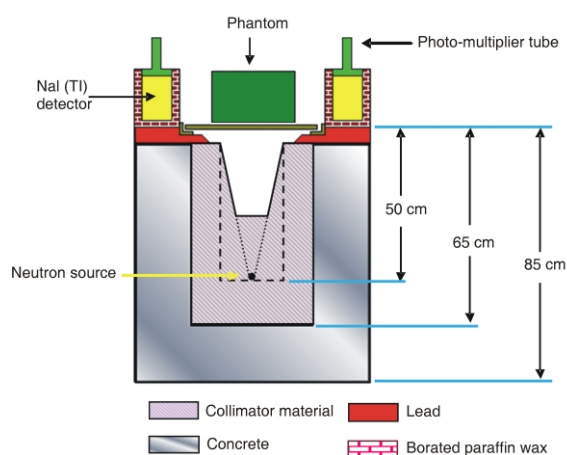


Figure 1. Schematic diagram of the prompt γ -rays IVNAA facility. The dotted lines show the pyramidal collimator void hole. The neutron source is placed at the apex, centrally under the phantom. The borders of the rectangular collimator void hole are represented with the dashed lines

Another shape of collimator studied in this work was composed of orthogonal parallelepiped void cast of $40 \times 20 \text{ cm}^2$ cross sectional area. The borders of the rectangular collimator void hole are represented with the dashed lines in fig 1. The neutron source position is fixed for both collimator shapes.

Monte Carlo simulations

MCNPX 2.4.0 code was used to simulate the IVNAA setup and estimate the dose and neutron fluxes. MCNP codes are general purpose, continuous energy, generalized geometry, coupled neutron/photon/electron, and time-dependent Monte Carlo transport codes. The cross-sections used in this project were chosen from the ENDF/B-VI libraries. Also, for neutrons below 4 eV, $S(\alpha, \beta)$ the scattering treatment was applied (MTm card).

The neutron energy spectrum of ^{252}Cf was assumed to be of a Watt distribution with the parameters $a = 1.025$ and $b = 2.926$ [16]. The ^{252}Cf prompt γ -rays spectrum was simulated, corresponding to the report Valentine [17]. The neutron energy spectrum of $^{241}\text{Am-Be}$ source was chosen from the IAEA report 403 [18]. The 4.43 MeV prompt γ -rays from $^{12}\text{C}^*$ were also considered.

The specific absorbed dose rate and specific ambient dose-equivalent rate were estimated for neutrons and photons by kerma assumption. In kerma approximation only the neutron and the neutron-induced photon transport is considered and the secondary charged particles are ignored (mode np). F6 tally (track length cell energy deposition tally) was employed for neutron and photon specific absorbed dose rate (pGy/h Bq) estimations. The specific ambient dose-equivalent rate (pSv/h Bq) was calculated using F4 tally (track length estimate of cell flux tally) modified by DE4 and DF4 cards (dose energy and dose function) according to conversion factors of ICRP74 [19].

The neutrons flux ($1/\text{cm}^2\text{s}$) and the production rate of neutron-induced photons ($1/\text{cm}^3\text{s}$) were assessed by the use of F4 neutron tally along with the E4 and appropriate FM4 multiplier cards, respectively.

RESULTS AND DISCUSSION

The main point in IVNAA method, especially for total body scanning, is the uniformity of the sample activation in the region of interest. So, the main aim of this work is the study on the uniformity in different setups. The data were compared on the basis of U index which was defined as the ratio of root mean square (rms) to the arithmetic mean of the estimated depth-distribution of gamma production rate (activation rate):

$$U = \frac{x_{rms}}{\bar{x}} \sqrt{1 + \frac{\sigma_x^2}{\bar{x}^2}}$$

where x_{rms} , \bar{x} , and σ_x are the rms, arithmetic mean, and the standard deviation of the depth-distribution of gamma production rate in the phantom, respectively.

If the desirable uniformity is obtained, then the dose data would be investigated. Tables 1 and 2 list the results of all unilateral setups for ^{252}Cf and $^{241}\text{Am-Be}$ neutron sources, respectively. The neutron and gamma specific ambient (H_n and H_g) and absorbed (D_n and D_g) dose rates together with the uniformity and thermal neutron flux in the exposed region of the phantom are recorded. For more information, the maximum to minimum ratio of gamma production rate values is listed as R in the uniformity column. In each table, two collimator shapes and four collimator materials are considered.

The preliminary calculations showed that by decreasing the collimator length from 45 cm, the thermal flux increased but the gamma production rate uniformity decreased. Moreover, the thermal neutron flux to dose ratio was not significantly changed. So, the 45 cm depth is considered for all collimator shapes and configurations.

All results in this work were estimated with the uncertainties less than 1%; therefore, the data errors are not shown in the tables and figures. These uncertainties are based on 150 million particles.

^{252}Cf and $^{241}\text{Am-Be}$ neutron sources

Figure 2 depicts the gamma production rate versus the depth of the sample in the small cells centered

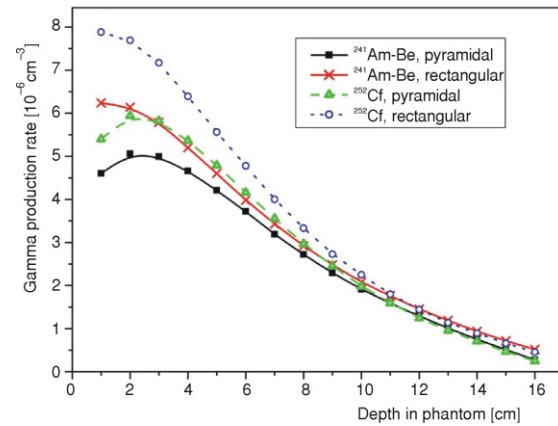


Figure 2. Gamma production rate vs. the depth of the sample for graphite material in the unilateral configuration

Table 1. Effect of collimator material and shape in unilateral configuration for $^{241}\text{Am-Be}$ source

| Collimator shape | Collimator material | Uniformity | | Specific absorbed dose rate [pGyh ⁻¹ Bq ⁻¹] | | Specific ambient dose equivalent rate [pSvh ⁻¹ Bq ⁻¹] | | $\Phi_{th} 10^{-5}$ [cm ⁻² s ⁻¹] | $\frac{\Phi_{th}}{H_T} 10^{-6}$ [cm ⁻² s ⁻¹ /pSvh ⁻¹ Bq ⁻¹] |
|------------------|---------------------|------------|-------|--|------|--|------|---|--|
| | | U | R | D_n | D | H_n | H | | |
| Pyramidal | CH ₂ -B | 1.10 | 9.32 | 2.68 | 1.06 | 30.60 | 1.11 | 4.15 | 1.31 |
| | CH ₂ | 1.14 | 12.67 | 2.67 | 1.43 | 30.97 | 1.50 | 5.31 | 1.63 |
| | C | 1.18 | 18.47 | 3.61 | 1.75 | 45.22 | 1.82 | 11.04 | 2.35 |
| | D ₂ O | 1.27 | 28.85 | 2.88 | 1.82 | 35.93 | 1.90 | 11.43 | 3.02 |
| Rectangular | CH ₂ -B | 1.17 | 9.82 | 2.62 | 1.40 | 32.06 | 1.48 | 7.39 | 2.20 |
| | CH ₂ | 1.24 | 15.39 | 2.61 | 1.88 | 32.60 | 1.96 | 8.97 | 2.60 |
| | C | 1.19 | 12.07 | 3.66 | 2.02 | 48.28 | 2.11 | 13.61 | 2.70 |
| | D ₂ O | 1.28 | 19.64 | 2.82 | 2.07 | 37.25 | 2.16 | 13.54 | 3.44 |

Table 2. Effect of collimator material and shape in unilateral configuration for ^{252}Cf source

| Collimator shape | Collimator material | Uniformity | | Specific absorbed dose rate [pGyh ⁻¹ Bq ⁻¹] | | Specific ambient dose equivalent rate [pSvh ⁻¹ Bq ⁻¹] | | $F_{th} 10^{-5}$ [cm ⁻² s ⁻¹] | $\frac{\Phi_{th}}{H_T} 10^{-6}$ [cm ⁻² s ⁻¹ /pSvh ⁻¹ Bq ⁻¹] |
|------------------|---------------------|------------|-------|--|------|--|------|--|--|
| | | U | R | D_n | D | H_n | H | | |
| Pyramidal | CH ₂ -B | 1.12 | 12.47 | 1.69 | 0.92 | 23.60 | 1.04 | 4.66 | 1.89 |
| | CH ₂ | 1.17 | 17.17 | 1.68 | 1.34 | 24.03 | 1.47 | 6.00 | 2.35 |
| | C | 1.21 | 24.15 | 2.29 | 1.65 | 35.54 | 1.78 | 12.45 | 3.34 |
| | D ₂ O | 1.29 | 36.46 | 1.78 | 1.75 | 28.17 | 1.89 | 12.51 | 4.16 |
| Rectangular | CH ₂ -B | 1.21 | 14.00 | 1.59 | 1.39 | 24.15 | 1.56 | 8.40 | 3.27 |
| | CH ₂ | 1.29 | 21.85 | 1.58 | 1.95 | 24.89 | 2.13 | 10.37 | 3.84 |
| | C | 1.23 | 17.36 | 2.37 | 2.10 | 38.79 | 2.29 | 16.03 | 3.90 |
| | D ₂ O | 1.32 | 26.27 | 1.72 | 2.15 | 29.11 | 2.34 | 15.51 | 4.93 |

above the source. The curves plotted in this figure include the activation rate for two neutron sources and two collimator shapes. The collimator material is graphite. As can be seen, $^{241}\text{Am-Be}$ shows the better uniformity than ^{252}Cf for both collimator shapes. Tables 1 and 2 also indicate that $^{241}\text{Am-Be}$ source has the advantage of better activation rate uniformity in comparison with ^{252}Cf source for other collimator materials. However, thermal neutron flux and then activation rates in all situations are higher for ^{252}Cf . Besides, the ambient and absorbed doses received by the phantom for $^{241}\text{Am-Be}$ are greater than for ^{252}Cf source.

Neutrons which are emitted from $^{241}\text{Am-Be}$ have higher energy than those of ^{252}Cf . These high neutrons guarantee the activation rate uniformity up to 8 cm depth. On the other hand, the significant part of the neutron absorbed dose is produced by the fast ones. Table 3 lists the normalized neutron fluxes (NNF) in exposed region of phantom for the four ICRP energy ranges: 0-0.01 MeV, 0.01-0.1 MeV, 0.1-2 MeV, and 2-20 MeV. Also, the normalized neutron absorbed doses (NAD) from these neutrons are recorded for four setups in fig. 2. Evidently, from this table, more than 96% of the neutron absorbed dose is due to fast neutrons (0.1-20 MeV) with less than 18% of neutron population, for all cases. The conversion factors for the ambient dose equivalent are greater for fast neutrons than for low energy neutrons. Therefore, fast neutrons are more effective for the ambient dose equivalent (which dominantly resulted more from neutrons than from photons) in comparison with the absorbed dose.

In other words, for the choice of the incident relative fast neutron flux, the compromise should be performed between the uniformity and the neutron dose. Nevertheless, due to the importance of activation uniformity with depth, $^{241}\text{Am-Be}$ source was chosen for the next setup designs in this study. Another advantage of $^{241}\text{Am-Be}$ neutron source is the long half-life of 342 years in comparison with 2.65 years of ^{252}Cf .

Collimator material

The collimator material is very effective on the incident neutron spectrum. It is observed from tabs. 1 and 2 that for both neutron sources and both pyrami-

dal and rectangular collimator shapes the activation rate is more uniform when borated-polyethylene is the collimator material. Polyethylene, graphite and heavy water are the next selections in the pyramidal shape. But for the rectangular configuration, graphite shows better uniformity than polyethylene. This is different from the report of Stamatelatos *et al.* [15] in which the graphite is the best choice. It probably depends on the sample size. In large samples, such as the phantom studied in this work, the thermal neutron flux and thereupon activation rate are sharply reduced, so that their values are nearly the same in deep regions for all situations and independent of the incident flux (see, for example, fig. 2). Therefore, increasing the incident thermal neutron flux increases the distance between thermal fluxes at the shallow and deep zones and so decreases the uniformity with depth, while the thermal neutron flux indeed increased with increasing the incident thermal flux up to 7-8 cm depth (small samples).

Although borated-polyethylene makes the activation rate curve more uniform in comparison with other materials, uniformity is not acceptable yet. Particularly, R values show that the activation rates in shallow and deep regions differ for the order of about 10.

Collimator shape: pyramidal and rectangular

The effect of the collimator shape is investigated in pyramidal and rectangular forms. The shape of collimator is effective on the estimated parameter in the phantom.

Tables 1 and 2 compare the rectangular and pyramidal forms in the unilateral configuration. For two neutron sources and two materials, borated-polyethylene and polyethylene, the switch from the pyramidal to rectangular configuration worsens U and R values. U values have the same manner toward graphite and heavy water, but slower. For R data this process is inverted.

Thermal neutron flux is increased when the rectangular shape is selected, for all cases. This situation could be due to the emitted neutrons which do not reach the collimator aperture directly. In the case of the rectangular shape, the collimator material can moder-

Table 3. Normalized neutron absorbed dose and relative number of neutrons in exposed region of phantom for graphite collimator material and unilateral configuration

| Interval [MeV] | $^{241}\text{Am-Be}$ Pyramidal | | $^{241}\text{Am-Be}$ Rectangular | | ^{252}Cf Pyramidal | | ^{252}Cf Rectangular | |
|----------------|--------------------------------|-------|----------------------------------|-------|-----------------------------|-------|-------------------------------|-------|
| | NAD | NNF | NAD | NNF | NAD | NNF | NAD | NNF |
| 0-0.01 | 0.003 | 0.790 | 0.003 | 0.811 | 0.005 | 0.839 | 0.006 | 0.858 |
| 0.01-0.1 | 0.017 | 0.029 | 0.018 | 0.028 | 0.029 | 0.030 | 0.032 | 0.028 |
| 0.1-2 | 0.302 | 0.089 | 0.337 | 0.086 | 0.509 | 0.091 | 0.538 | 0.082 |
| 2-20 | 0.679 | 0.091 | 0.642 | 0.076 | 0.458 | 0.040 | 0.424 | 0.032 |

ate such neutrons and also reflect them toward the body, while there is a small probability that these neutrons can escape from the collimator material if the collimator shape is pyramidal.

The neutron and gamma specific ambient dose equivalent rates and gamma absorbed doses are greater for the rectangular than pyramidal shape, while neutron specific absorbed dose rates, except for graphite, are higher for the pyramidal shape. In spite of the ambient dose equivalent increment, thermal neutron flux to total ambient dose equivalent ratios increase during the conversion from the pyramidal to rectangular form.

Up to now, for the unilateral configuration, borated-polyethylene in pyramidal collimator has the best activation rate uniformity with $U = 1.1$. However, it is not sufficient for the precise IVNAA experiments.

Unilateral or bilateral configuration

Figure 2 represents another point: the gamma production rate decreases to about half of its preliminary value (1 cm depth) exactly in the middle of the sample. Then, at the end (16 cm depth), the gamma production rate is less than 10% of the preliminary value. This decline process induces the use of the bilateral schema, because the outcome is very uniform if the curve of the gamma production rate vs. depth adds to its inverse (using the same setup at the other side). However, the conditions of the superposition principal are not completely established in this discussion.

The new MCNP runs were performed for the bilateral configuration and two $^{241}\text{Am-Be}$ neutron sources. These results are listed in tab. 4, in the format of tabs. 1 and 2. Four collimator materials and two shapes are investigated. To compare the data in tabs. 1 and 4 just upon facility configuration (unilateral/bilateral), the estimations are performed for one neutron emitted per second from both sources. The results can be summarized as follows:

- the pyramidal shape presents more uniform activation rate distribution with depth,

- borated polyethylene shows the better uniformity of the activation rate, followed by graphite, polyethylene, and heavy water. However, there is a little advantage of borated polyethylene over graphite,
- for R data, graphite has smaller values compared with borated polyethylene,
- the neutron dose data are the same as unilateral cases (the similar situations in tabs. 1 and 4). This is reasonable because fast neutron flux which has a dominant role in neutron doses is approximately the same for two configurations,
- similar to tabs. 1 and 2, gamma absorbed doses are of the order of the neutron absorbed doses in all cases, while the ambient dose equivalents come from neutrons more significantly than from photons,
- the rectangular configuration presents greater thermal neutron flux and dose data. The thermal neutron flux to specific ambient dose equivalent rate ratio is higher in the rectangular shape because the thermal neutron flux increases more rapidly than the specific ambient dose equivalent rate through switching from the pyramidal to rectangular configuration, and
- though, the specific ambient dose equivalent rate is higher for graphite, thermal neutron flux to the specific ambient dose equivalent rate ratio is the biggest one after heavy water data. It is due to the great thermal neutron flux when graphite is a collimator material. Thermal neutron flux is greater for graphite than borated polyethylene by the factor of 2 in both pyramidal and rectangular forms. These data for thermal neutron flux to the specific ambient dose equivalent rate ratio are about 1.4 and 1.2 for the pyramidal and rectangular forms, respectively.

Figure 3 depicts the gamma production rate versus the depth of the sample for the bilateral configuration. Two collimator materials (borated polyethylene and graphite) and two collimator shapes (pyramidal and rectangular) are considered.

It seems that the graphite is the best choice for the collimator material because of the very good uni-

Table 4. Effect of collimator material and shape in bilateral configuration for $^{241}\text{Am-Be}$ source

| Collimator shape | Collimator material | Uniformity | | Specific absorbed dose rate [pGyh ⁻¹ Bq ⁻¹] | | Specific ambient dose equivalent rate [pSvh ⁻¹ Bq ⁻¹] | | $\Phi_{\text{th}} 10^{-5}$ [cm ⁻² s ⁻¹] | $\frac{\Phi_{\text{th}}}{H_{\text{T}}} 10^{-6}$ [cm ⁻² s ⁻¹ /pSvh ⁻¹ Bq ⁻¹] |
|------------------|---------------------|------------|-------|--|------|--|------|--|--|
| | | U | R | D_{n} | D | H_{n} | H | | |
| Pyramidal | CH ₂ -B | 1.002 | 1.190 | 2.75 | 1.29 | 32.23 | 1.36 | 5.79 | 1.72 |
| | CH ₂ | 1.008 | 1.418 | 2.72 | 1.64 | 32.36 | 1.71 | 6.71 | 1.97 |
| | C | 1.002 | 1.185 | 3.47 | 1.83 | 43.59 | 1.91 | 11.22 | 2.47 |
| | D ₂ O | 0.013 | 1.533 | 2.91 | 1.86 | 36.23 | 1.94 | 10.88 | 2.85 |
| Rectangular | CH ₂ -B | 1.003 | 1.251 | 2.92 | 1.56 | 35.75 | 1.65 | 8.33 | 2.23 |
| | CH ₂ | 1.017 | 1.648 | 2.88 | 2.05 | 36.10 | 2.15 | 10.14 | 2.65 |
| | C | 1.004 | 1.240 | 4.19 | 2.21 | 55.23 | 2.31 | 15.41 | 2.68 |
| | D ₂ O | 1.023 | 1.785 | 3.14 | 2.26 | 41.67 | 2.36 | 15.41 | 3.50 |

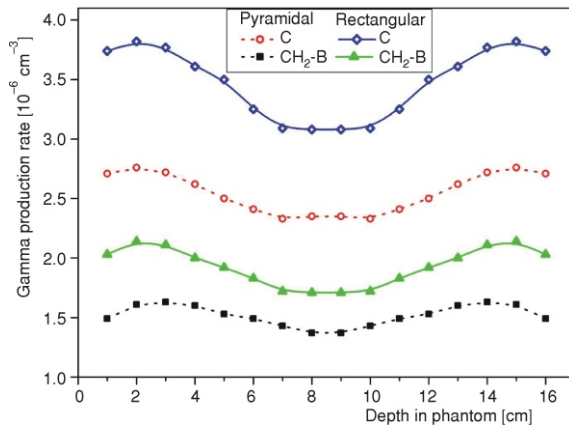


Figure 3. Gamma production rate vs. the depth of the sample for $^{241}\text{Am-Be}$ source in bilateral configuration

formity (in the pyramidal shape, the best one) and the high thermal neutron flux to dose ratio. The pyramidal form shows the better uniformity, but with a little risk in uniformity the rectangular shape can decrease the scan time due to higher thermal neutron flux and the ratio of it to the dose. So, the bilateral pyramidal collimator shape with graphite as a collimator material and $^{241}\text{Am-Be}$ as a neutron source is suggested for an IVNAA facility, especially in total body counting. This situation with the rectangular shape has a little decline in uniformity (about 0.2% in U) with about 9% increment in the thermal neutron flux to dose ratio.

CONCLUSIONS

This paper studies the effects of the neutron source type and collimator material and shape on the uniformity of the activation rate distribution with depth in a large biological sample. The dose calculations are also performed for the specific absorbed dose rate and the specific ambient dose equivalent rate.

The $^{241}\text{Am-Be}$ neutron source, due to its wide fast neutron spectrum, is recommended to improve the uniformity. Borated polyethylene as a collimator material presents the best uniformity (the least U) in all situations. The pyramidal collimator shape has better results of uniformity (U and R) in comparison with the rectangular form, in all cases. Unilateral forms do not show acceptable uniform curves of the activation rate with depth, so this form is not suggested, particularly for total body scanning. Evidently, the bilateral form, as expected, gets desirable U values for borated polyethylene and graphite collimator materials. The bilateral shape is necessary for total body scans. In the bilateral shape, graphite as a collimator material presents the uniformity as good as borated polyethylene, while the thermal neutron flux and its ratio to the specific ambient dose equivalent rate are higher for graphite.

So, the graphite is selected as the collimator material. Between the pyramidal and rectangular forms with graphite collimator material, one can choose the rectangular shape with the acceptance of about 0.2% deterioration in U instead of 9% increment in the thermal neutron flux to dose ratio.

FUNDING

This study was funded by the Vice President for Research & Technology of Ferdowsi University of Mashhad, Iran.

REFERENCES

- [1] Sutcliffe, J. F., A Review of *in vivo* Experimental Methods to Determine the Composition of the Human Body, *Physics in Medicine and Biology*, 41 (1996), 5, pp. 791-833
- [2] Evans, H. J., Leblanc, A. D., Johnson, P. C., Facility for Regional *in vivo* Neutron Activation Analysis of Skeletal Calcium, *Physics in Medicine and Biology*, 24 (1979), 1, pp. 181-187
- [3] Ma, R., Ellis, K. J., Yasumura, S., Shypailo, R. J., Pierson, R. N., Total Body-Calcium Measurements: Comparison of Two Delayed-Gamma Neutron Activation Facilities, *Physics in Medicine and Biology*, 44 (1999) 6, pp. N113-N118
- [4] O'Meara, J. M., Blackburn, B. W., Chichester, D. L., Gierga, D. P., Yanch, J. C., The Feasibility of Accelerator-Based *in vivo* Neutron Activation Analysis of Nitrogen, *Applied Radiation and Isotopes*, 55 (2001), 6, pp. 767-774
- [5] Chichester, D. L., Empey, E., Measurement of Nitrogen in the Body Using a Commercial PGNA System-Phantom Experiments, *Applied Radiation and Isotopes*, 60 (2004), 1, pp. 55-61
- [6] Kasviki, K., Stamatelatos, I. E., Yannakopoulou, E., Papadopoulou, P., Kalef-Ezra, J., On the Accuracy of Protein Determination in Large Biological Samples by Prompt Gamma Neutron Activation Analysis, *Nuclear Instruments and Methods in Physics Research Section B, Beam Interactions with Materials and Atoms*, 263 (2007), 1, pp. 132-135
- [7] Kasviki, K., Stamatelatos, I. E., Kalef-Ezra, J., Evaluation of Spatial Sensitivity of a Prompt Gamma Neutron Activation Analysis Facility for the *in vivo* Determination of Nitrogen in Small Animals, *Journal of Radioanalytical and Nuclear Chemistry*, 271 (2007), 1, pp. 225-231
- [8] Mernagh, J. R., Harrison, J. E., McNeill, K. G., *In vivo* Determination of Nitrogen Using Pu-Be Sources, *Physics in Medicine and Biology*, 22 (1977), 5, pp. 831-835
- [9] Mattsson, S., Thomas, B. J., Development of Methods for Body Composition Studies, *Physics in Medicine and Biology*, 51 (2006), 13, pp. R203-228
- [10] Franklin, D. M., Armstrong, R., Chettle, D. R., Scott, M. C., An Improved *in vivo* Neutron Activation System for Measuring Kidney Cadmium, *Physics in Medicine and Biology*, 35 (1990), 10, pp. 1397-1408
- [11] Atanackovic, J., Grinyer, J., Chettle, D. R., Byun, S. H., The Comparison of Two MCNP Models Used for Prompt Gamma *in vivo* Detection of Cadmium and

- Mercury, *Nuclear Instruments and Methods in Physics Research Section B, Beam Interactions with Materials and Atoms*, 263 (2007), 1, pp. 169-174
- [12] Elliott, A., Holloway, I., Boddy, K., Haywood, J. K., Williams, D., Neutron Uniformity Studies Related to Clinical Total Body *in vivo* Neutron Activation Analysis, *Physics in Medicine and Biology*, 23 (1978), 2, pp. 269-281
- [13] Krishnan, S. S., McNeill, K. G., Mernagh, J. R., Bayley, A. J., Harrison, J. E., Improved Clinical Facility for *in vivo* Nitrogen Measurement, *Physics in Medicine and Biology*, 35 (1990), 4, pp. 489-499
- [14] Boddy, K., Elliott, A., Robertson, I., Mahaffy, M. E., Holloway, I., A High Sensitivity Dual-Detector Shadow-Shield Whole-Body Counter with an 'Invariant' Response for Total Body *in vivo* Neutron Activation Analysis, *Physics in Medicine and Biology*, 20 (1975), 2, pp. 296-304
- [15] Stamatelatos, I. E., Kasviki, K., Green, S., Gainey, M., Kalef-Ezra, J., Beddoe, A., Prompt-Gamma Neutron Activation Analysis Facility for *in vivo* Body Composition Studies in Small Animals, *Analytical and Bioanalytical Chemistry*, 379 (2004), 2, pp. 192-197
- [16] ***, MCNPX™ User's Manual, Version 2.4.0. (Ed. L. Waters), Los Alamos National Laboratory Report LACP-02-408, Los Alamos, N. Mex., USA, 2002
- [17] Valentine, T. E., Evaluation of Prompt Fission Gamma Rays for Use in Simulating Nuclear Safeguard Measurements, *Annals of Nuclear Energy*, 28 (2001), 3, pp. 191-201
- [18] ***, Compendium of Neutron Spectra and Detector Responses for Radiation Protection Purposes – Supplement to Technical Report Series No. 318, Technical Report Series No. 403, International Atomic Energy Agency, Vienna, 2001
- [19] ***, ICRP Publication 74, Conversion Coefficients for Use in Radiological Protection Against External Radiation, International Commission on Radiological Protection, Published by Elsevier Health Sciences, Pergamon Press, Oxford, UK, 1996

Хашем Мири ХАКИМАБАД, Лале Рафат МОТАВАЛИ

ПОБОЉШАЊЕ УНИФОРМНОСТИ РАСПОДЕЛЕ ПРОИЗВЕДЕНОГ ГАМА ЗРАЧЕЊА ПО ДУБИНИ ВЕЛИКОГ БИОЛОШКОГ УЗОРКА У IVNAA ПОСТРОЈЕЊУ

У раду су описане пројектне студије које се односе на тренутно гама зрачење у постројењу за *ин виво* неутронску активациону анализу. Пројектовање се заснивало на ^{252}Cf и ^{241}Am -Ве неутронским изворима и на четири колиматорска материјала: полиетилену, полиетилену натопљеном 5% борном киселином, графиту и тешкој води; такође, на пирамидалном и ректангуларном облику колиматора у унилатералној и билатералној конфигурацији. Циљ рада је био да се побољша униформност расподеле интензитета произведеног гама зрачења по дубини великог биолошког узорка. Као узорак, симулиран је водени фантом димензије 32 cm 16 cm 100 cm. Симулација је обављена MCNPX 2.4.0 Монте Карло кодом. Проучавање је препоручило IVNAA постројење са тренутним гама зрачењем, билатералне конфигурације са графитним колиматором и ^{241}Am -Ве неутронским извором.

Кључне речи: производња гама зрачења, водени фантом, MCNPX код, активациона анализа